

# Exploring the [S/Fe] Behavior of Metal-Poor Stars with the S I 1.046 $\mu\text{m}$ Lines \* †

Yoichi TAKEDA

*National Astronomical Observatory of Japan 2-21-1 Osawa, Mitaka, Tokyo 181-8588*  
*takeda.yoichi@nao.ac.jp*

and

Masahide TAKADA-HIDAI

*Liberal Arts Education Center, Tokai University, 1117 Kitakaname, Hiratsuka, Kanagawa 259-1292*  
*hidai@apus.rh.u-tokai.ac.jp*

(Received 2010 July 29; accepted 2010 August 23)

## Abstract

In an attempt of clarifying the [S/Fe] behavior with the run of [Fe/H] in the metal-poor regime which has been a matter of debate, an extensive non-LTE analysis of near-IR S I triplet lines (multiplet 3) at 1.046  $\mu\text{m}$  was carried out for selected 33 halo/disk stars in a wide metallicity range of [Fe/H]  $\sim -3.7$  to  $\sim +0.3$ , based on the spectral data collected with IRCS+AO188 of the Subaru Telescope. We found an evidence of considerably large [S/Fe] ratio amounting to  $\sim +0.7$ – $0.8$  dex at very low metallicity of [Fe/H]  $\sim -3$ , which makes marked contrast with other  $\alpha$ -elements (Mg, Si, Ca, Ti) flatly showing moderately supersolar [ $\alpha$ /Fe] of  $\sim 0.3$  dex. Meanwhile, a locally-flat tendency of [S/Fe] at  $\sim +0.3$  is seen at  $-2.5 \lesssim [\text{Fe}/\text{H}] \lesssim -1.5$ . These results may suggest that the nature of [S/Fe] in metal-poor halo stars is not so simple as has been argued (i.e., neither being globally flat independent of [Fe/H] nor monotonically increasing with a decrease in [Fe/H]), but rather complicated with a local plateau around [Fe/H]  $\sim -2$  followed by a discontinuous jump between the narrow interval of  $-3 \lesssim [\text{Fe}/\text{H}] \lesssim -2.5$ .

**Key words:** stars: abundances — stars: atmospheres — stars: late-type  
– stars: Population II

## 1. Introduction

Sulfur belongs to the important group of  $\alpha$ -capture elements, whose abundances in very metal-poor stars play a key role for studying the galactic chemical evolution, because most of them are considered to have been synthesized in short-lived massive stars and thrown out by type II supernovae at the early history of the Galaxy. Among these, S (along with O) deserves a particular attention because of its chemically “volatile” nature; i.e., it is difficult to condense into solid owing to its low condensation temperature ( $T_c \sim 650$  K) unlike other “refractory”  $\alpha$  group (Mg, Si, Ca, Ti) with high  $T_c$  of  $\sim 1300$ – $1500$  K. This fact characterizes the S abundances of metal-deficient stars as a reliable probe for the  $\alpha$ -chemistry of old galactic gas because S atoms synthesized and emitted by SNe II are directly circulated into the gas (from which stars form), in contrast to other refractory species which might have at first fractionated onto dust and later deposited to the gas after a considerable elapse of time (time-delayed deposition; e.g., Ramaty et al. 2001). For this reason, it is of paramount importance to establish the run of [S/Fe] with a change of [Fe/H] in very metal-poor stars.

Unfortunately, however, no consensus has yet been accomplished regarding the behavior of [S/Fe] of old halo stars, since two abundance indicators (S I 8693–4 lines of multiplet 6 and S I 9212/9228/9237 lines of multiplet 1), which have been mainly used to trace the S abundances of metal-poor stars, tend to yield discordant results in the very low metallicity regime: The former suggested an ever-increasing [S/Fe]<sub>86</sub> with a decrease of [Fe/H] up to [S/Fe]<sub>86</sub>  $\sim +0.8$  at [Fe/H]  $\sim -2.5$  (“rising” tendency; cf. Israelian & Rebolo 2001; Takada-Hidai et al. 2002), while the latter resulted in a trend of nearly constant [S/Fe]<sub>92</sub> at a mildly supersolar value of  $\sim +0.3$ – $0.5$  irrespective of the metallicity down to [Fe/H]  $\sim -3$  (“flat” tendency; cf. Ryde & Lambert 2004; Nissen et al. 2004; Takada-Hidai et al. 2005; Takada-Hidai & Sargent 2005). Since all these studies on [S/Fe]<sub>92</sub> invoked the assumption of LTE, Takeda et al. (2005b) investigated the non-LTE effect on abundance determinations from S I 9212/9228/9237 lines and found appreciable “negative” corrections<sup>1</sup> amounting to  $\sim 0.2$ – $0.3$  dex, which embarrassingly makes the discrepancy between [S/Fe]<sub>86</sub> and [S/Fe]<sub>92</sub> even larger. While Nissen et al. (2007b, 2008) concluded by taking into account the non-LTE effect that galactic halo stars dis-

\* Based on data collected at Subaru Telescope, which is operated by the National Astronomical Observatory of Japan.

† The large data tables are separately provided in the machine-readable form as electronic tables E1 and E2.

<sup>1</sup> The significance of downward non-LTE corrections for these multiplet 1 lines has also been confirmed by recent non-LTE calculations done by Korotin (2009), who derived results similar to those of Takeda et al. (2005b).

tribute around a plateau of  $[S/Fe]_{92} \sim +0.2-0.3$  like other  $\alpha$ -elements, the controversial “flat vs. increasing” debate depending on different abundance indicators has not yet been settled. Do two populations showing different  $[S/Fe]$  behaviors (high- and low- $[S/Fe]$ ) exist in the metal-poor regime, as suggested by Caffau et al. (2005)?

From a viewpoint of reliability, each of these two S abundance indicators actually have specific shortcomings: Although S I 8693–4 lines are well-behaved in the sense that they are insensitive to the non-LTE effect as well as the microturbulence, their strengths are not so large to be reliably usable for very metal-poor stars at  $[Fe/H] \lesssim -2$ . In contrast, S I 9212/9228/9237 lines are sufficiently strong as to be invoked for studying  $[S/Fe]$  in the metallicity range down to  $[Fe/H] \sim -3$ . Unfortunately, however, they are located in a spectral region considerably contaminated by a jungle of telluric  $H_2O$  lines, which (despite any effort of elimination) may seriously affect the accuracy of *EW* measurements for very weak lines.

Considering this situation, Takeda et al. (2005b) proposed an alternative use of S I triplet lines of multiplet 3 (4p  $^5P - 4d \ ^5D^\circ$ ) at 10455–10459 Å for exploring  $[S/Fe]$  of metal-poor stars, which are nearly as strong as S I 9212/9228/9237 lines and locate in a region almost free from any contamination of telluric lines; thus being certainly advantageous compared to the other two. Therefore, it is interesting to see which kind of  $[S/Fe]$  trend would result from these 10455–9 lines. As far as we know, however, only a limited studies on  $[S/Fe]$  of metal-poor stars has been carried out so far with these near-IR lines: While the first report for G 29-23 ( $[Fe/H] = -1.7$ ) was made by Nissen et al. (2007a, b), Caffau et al. (2010) recently published the results for four stars (BD−05°3640, HD 140283, HD 181743, and HD 211998) ranging from  $[Fe/H] \sim -1.2$  to  $\sim -2.4$ , both being based on VLT/CRIRES spectra. Although these studies derived  $[S/Fe]$  ratios to be in the range of  $+0.3-0.7$ , this sample is still too small, and a more extensive investigation is evidently needed for any statistically meaningful information.

Hence, we decided to investigate this controversial situation on the  $[S/Fe]$  vs.  $[Fe/H]$  trend of metal-deficient stars by ourselves with these S I 10455–10459 lines. Toward this aim, we secured moderately high-dispersion spectra in *zJ*-band for 33 stars of various metallicity in 2009 July by using IRCS+AO188 of the Subaru Telescope. The purpose of this paper is to report the sulfur abundances of these stars resulting from our analysis.

The remainder of this article is organized as follows. After describing the observational data (section 2) and stellar parameters (section 3) of the target stars, we explain the details of abundance determinations in section 4, followed by the discussion (section 5) where the results are presented and examined in comparison with the published work. The conclusion is summarized in section 6, followed by an Appendix where the nature of HD 219617 (double-star system comprising similar components) is briefly mentioned.

## 2. Observational Data

We selected 33 targets of halo/disk stars in the metallicity range of  $-3.7 \lesssim [Fe/H] \lesssim +0.3$ , for which published atmospheric parameters are available. While our halo sample ( $[Fe/H] \lesssim -1$ ) comprises dwarfs as well as giants, most of the disk targets ( $-1 \lesssim [Fe/H]$ ) are dwarfs. The list of the program stars is presented in table 1.

The observations were conducted on 2009 July 29 and 30 (UT) by using the Infrared Camera and Spectrograph (IRCS; Kobayashi et al. 2000; Tokunaga et al. 1998) along with the 188-element curvature-based adaptive optics system (AO188), which is mounted on the IR Nasmyth focus of the 8.2 m Subaru Telescope atop Mauna Kea. The *zJ*-band (1.04–1.19  $\mu m$ ) spectra were taken in the echelle spectrograph mode of IRCS, which is equipped with a Raytheon 1024×1024 InSb array with an Aladdin II multiplexer. We used a very narrow slit of  $0.''14 \times 3.''47$  in order to accomplish the highest spectral resolution of  $R \simeq 20000$ . Thanks to the effective adaptive optics system (where the target itself was used as the guide star) enabling to reduce the size of stellar image down to FWHM  $\lesssim 0.''1$  irrespective of natural seeing condition, stellar photons could be efficiently collected even in such a narrow slit. Actual exposures were done in two different positions (A and B) by shifting the image in the direction of the slit length and one observation cycle consisted of an A-B-B-A sequence of four exposures. The time for one (A or B) exposure was from one second (at the shortest) to 15 minutes (at the longest) depending on the brightness. Several cycles were repeated for a star according to the necessity to achieve a sufficient S/N ratio. For two very metal-poor stars of special interest (BD+44°493 and G 64-37), we expended comparatively long total exposure times of  $\sim 1$  hr.

The reduction of the spectra (A–B subtraction for background cancellation, flat-fielding, bad-pixel correction, cosmic-ray events correction, scattered-light subtraction, aperture extraction, wavelength calibration, co-adding of spectrum frames, and continuum normalization) was performed by using the “echelle” package of the software IRAF<sup>2</sup> in a standard manner. For most of the targets, sufficiently high S/N ratios of  $\sim 100-200$  ( $S/N \sim 300$  for BD+44°493) were eventually accomplished. We confirmed by inspecting the line width that the expected spectral resolving power of  $R \sim 20000$  is actually attained.

## 3. Stellar Parameters

### 3.1. Atmospheric Parameters

Regarding the atmospheric parameters ( $T_{\text{eff}}$ ,  $\log g$ ,  $v_t$ , and  $[Fe/H]$ ) of the program stars necessary for constructing model atmospheres and determining abundances, various published studies were consulted. In case where two or more choices were possible, we preferentially selected

<sup>2</sup> IRAF is distributed by the National Optical Astronomy Observatories, which is operated by the Association of Universities for Research in Astronomy, Inc. under cooperative agreement with the National Science Foundation.

spectroscopically determined ones. The finally adopted parameter values (with the references) are presented in table 1. As seen from the  $T_{\text{eff}}$  vs.  $\log g$  diagram shown in figure 1a, our targets are roughly divided, according to the surface gravity, into dwarfs ( $\log g > 3$ ) and giants ( $\log g < 3$ ). Also noted from this figure is the trend of  $\log g$  tending to be lower with decreasing  $T_{\text{eff}}$ .

### 3.2. Kinematic Properties

In order to examine the kinematic properties of the program stars, we computed their orbital motions within the galactic gravitational potential based on the positional and proper-motion data (taken from SIMBAD database) along with the radial-velocity data (measured from our spectra), following the procedure described in subsection 2.2 of Takeda (2007). The adopted input data and the resulting solutions of kinematic parameters (space velocity components, orbital eccentricity, mean galactocentric radius, etc.) are summarized in electronic table E1. Figures 1b–d show the mutual correlations of  $z_{\text{max}}$  (maximum separation from the galactic plane),  $V_{\text{LSR}}$  (tangential component of the space velocity relative to the Local Standard of Rest), and  $[\text{Fe}/\text{H}]$  (metallicity). Applying Ibukiyama and Arimoto’s (2002) classification criteria (cf. figure 1b), we can roughly divide our targets from these figures that  $\sim 50\%$ ,  $\sim 20\%$ , and  $\sim 30\%$  belong to halo population with  $[\text{Fe}/\text{H}] \lesssim -1$ , thick-disk population with  $-1 \lesssim [\text{Fe}/\text{H}] \lesssim -0.5$ , and thin-disk population with  $-0.5 \lesssim [\text{Fe}/\text{H}]$ , respectively.

## 4. Abundance Determination

### 4.1. Synthetic Spectrum Fitting

We interpolated Kurucz’s (1993) grid of ATLAS9 model atmospheres<sup>3</sup> as well as the grid of the non-LTE departure coefficients computed by Takeda et al. (2005b) in terms of  $T_{\text{eff}}$ ,  $\log g$ , and  $[\text{Fe}/\text{H}]$  to generate the atmospheric model

<sup>3</sup> These ATLAS9 models computed by Kurucz (1993) approximately include the convective overshooting effect in an attempt to simulate the real convection as possible. It has been occasionally argued, however, that this treatment may cause inconsistencies with observational quantities (e.g., colors or Balmer line profiles) and even the classical pure mixing-length treatment “without overshooting” would be a better choice (e.g., Castelli et al. 1997). Since lines tend to become somewhat weaker in “with overshooting” atmospheres as compared to “without overshooting” cases because of the lessened temperature gradient in the lower part of the atmosphere, some difference may be expected in resulting abundances between these two cases, especially for comparative higher  $T_{\text{eff}}$  stars (i.e., early G to late A; cf. Fig. 24 of Castelli et al.) where the convection zone due to hydrogen ionization comes close to the bottom of the atmosphere. We investigated how much S abundance difference would result in the analysis of S I 10455–10459 lines when “without overshooting” models were used instead of “with overshooting” ones. Test calculations for the representative case of  $T_{\text{eff}} = 6000$  K and  $\log g = 4.0$  (for  $[\text{Fe}/\text{H}] = 0$  and  $-3$ ) revealed, however, that the abundance differences are only  $\lesssim 0.05$  dex (i.e., slightly lower abundances are obtained when the overshooting option is switched off). Accordingly, we may conclude that the difference of how the convection is treated is insignificant in the present case.

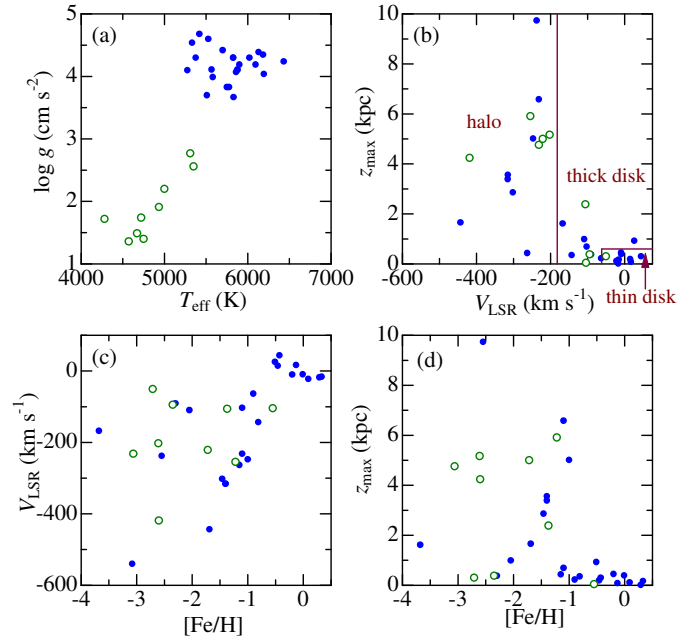


**Fig. 1.** Correlations of representative stellar parameters. Filled (blue) and open (green) symbols indicate dwarfs ( $\log g > 3$ ) and giants ( $\log g < 3$ ), respectively. (a)  $T_{\text{eff}}$  vs.  $\log g$ , (b)  $V_{\text{LSR}}$  vs.  $z_{\text{max}}$ , (c)  $[\text{Fe}/\text{H}]$  vs.  $V_{\text{LSR}}$ , and (d)  $[\text{Fe}/\text{H}]$  vs.  $z_{\text{max}}$ . Note that, one star (G 64-37) is not plotted in panels (b) and (d), since its  $z_{\text{max}}$  turned out abnormally large and unreliable.

and the departure coefficient data for each star.

Then we carried out non-LTE spectrum-synthesis analyses by applying Takeda’s (1995) automatic fitting procedure to the region of S I 10455–10459 lines while regarding the sulfur abundance as well as the macro-broadening parameter and the radial velocity as adjustable parameters to be established. The adopted atomic data of the relevant S I lines are presented in table 2. How the theoretical spectrum for the converged solutions fits well with the observed spectrum is displayed in figure 2, and the resulting non-LTE S abundances ( $A^N$ ) are given in table 1. Regarding the Sun, we obtained  $A_{\odot}^N = 7.20$  based on Kurucz et al.’s (1984) solar flux spectrum, which was used as the reference solar sulfur abundance. Accordingly, we evaluated  $[\text{S}/\text{H}]$  and  $[\text{S}/\text{Fe}]$  values for each star as  $[\text{S}/\text{H}] \equiv A^N - 7.20$  and  $[\text{S}/\text{Fe}] \equiv [\text{S}/\text{H}] - [\text{Fe}/\text{H}]$ .

As to BD+44°493, the most metal-poor star among our sample ( $[\text{Fe}/\text{H}] \sim -3.7$ ), we unfortunately could not detect any trace of S I lines in our spectrum (cf. figure 2) in spite of its fairly high S/N ratio ( $\sim 300$ ). We therefore estimated the upper limit of equivalent width for the strongest component at 10455.45 Å as  $EW_{10455}^{\text{UL}} \simeq k \times \text{FWHM}/(\text{S/N}) \simeq 4$  mÅ, where  $k$  is a factor we assumed to be 2 according to our experience and FWHM was set to 0.6 Å (estimated from the width of the C I line at 10691 Å). By using this  $EW_{10455}^{\text{UL}}$  and following the procedure described in the next subsection, we derived  $A^N \leq$

4.49 (with  $\Delta_{10455} = -0.34$ ) or  $[S/Fe] \leq +0.96 (\simeq +1.0)$  for this star.

#### 4.2. Abundance-Related Quantities

While the non-LTE synthetic spectrum fitting directly yields the final abundance solution, this approach is not necessarily suitable when one wants to evaluate the extent of non-LTE corrections or to study the abundance sensitivity to changing the atmospheric parameters (i.e., it is tedious to repeat the fitting process again and again for different assumptions or different atmospheric parameters). Therefore, with the help of Kurucz’s (1993) WIDTH9 program (which had been considerably modified in various respects; e.g., inclusion of non-LTE effects, etc.), we computed the equivalent widths for each of the triplet lines ( $EW_{10455}$ ,  $EW_{10456}$ , and  $EW_{10459}$ ) “inversely” from the abundance solution (resulting from non-LTE spectrum synthesis) along with the adopted atmospheric model/parameters, since they are much easier to handle. Based on such evaluated  $EW$  values, the LTE abundances for each of the lines ( $A_{10455}^L$ ,  $A_{10456}^L$ , and  $A_{10459}^L$ ) were freshly computed, from which the non-LTE corrections ( $\Delta_{10455}$ ,  $\Delta_{10456}$ , and  $\Delta_{10459}$ ) were derived such as  $\Delta_{10455} \equiv A_{10455}^L - A^N$ , etc.

We then estimated the uncertainties in  $A^N$  by repeating the analysis on  $EW_{10455}$  ( $EW$  for the strongest component) while perturbing the standard values of atmospheric parameters interchangeably by  $\pm 100$  K in  $T_{\text{eff}}$ ,  $\pm 0.2$  dex in  $\log g$ , and  $\pm 0.3$  km s $^{-1}$  in  $v_t$  (which we regarded as typical uncertainties of the atmospheric parameters according to the original references). Let us call these six kinds of abundance variations as  $\delta_{T+}$ ,  $\delta_{T-}$ ,  $\delta_{g+}$ ,  $\delta_{g-}$ ,  $\delta_{v+}$ , and  $\delta_{v-}$ , respectively. We then computed the root-sum-square of three quantities  $\delta_{T_{gv}} \equiv (\delta_{T+}^2 + \delta_{T-}^2 + \delta_v^2)^{1/2}$  as the abundance uncertainty (due to combined errors in  $T_{\text{eff}}$ ,  $\log g$ , and  $v_t$ ), where  $\delta_T$ ,  $\delta_g$ , and  $\delta_v$  are defined as  $\delta_T \equiv (|\delta_{T+}| + |\delta_{T-}|)/2$ ,  $\delta_g \equiv (|\delta_{g+}| + |\delta_{g-}|)/2$ , and  $\delta_v \equiv (|\delta_{v+}| + |\delta_{v-}|)/2$ , respectively.<sup>4</sup>

The resulting  $[S/Fe]$ ,  $\Delta_{10455}$ , and  $EW_{10455}$  for each star are plotted against  $T_{\text{eff}}$  in figures 3a–c, where the error bar attached to  $[S/Fe]$  represents  $\delta_{T_{gv}}$ . We can see from these figures that  $-0.4 \lesssim \Delta_{10455} \lesssim 0$  and  $10 \text{ m}\AA \lesssim EW_{10455} \lesssim 160 \text{ m}\AA$ , with a characteristic  $[Fe/H]$ -dependence differing between dwarfs and giants. While only representative  $A^N$ ,  $EW_{10455}$ ,  $\Delta_{10455}$ , and  $[S/Fe]$  are given in table 1, all the

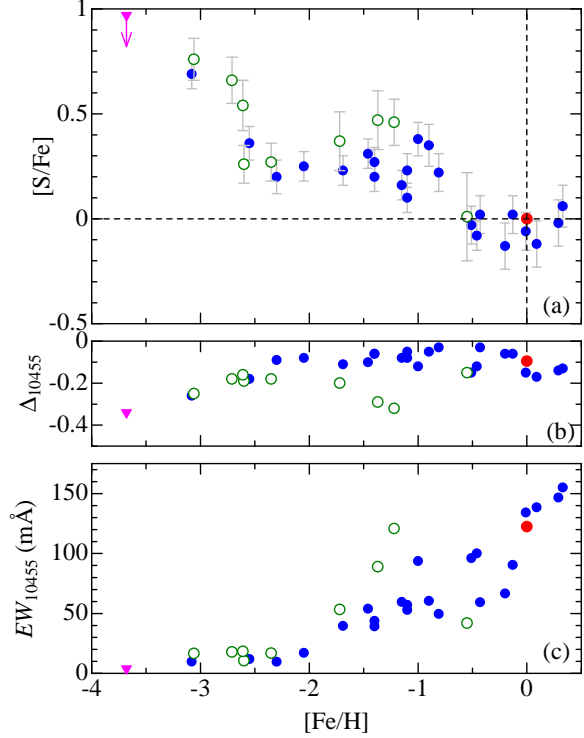


**Fig. 3.** Sulfur abundances (along with the related quantities) plotted against  $[Fe/H]$ : (a)  $[S/Fe]$  (S-to-Fe logarithmic abundance ratio corresponding to non-LTE sulfur abundance; where attached error bars represent the ambiguities due to uncertainties in the atmospheric parameters ( $\delta_{T_{gv}}$ ; cf. subsection 4.2) (b)  $\Delta_{10455}$  (non-LTE correction for the S I 10455 line). (c)  $EW_{10455}$  (equivalent width for the S I 10455 line). Dwarfs ( $\log g > 3$ ) and giants ( $\log g < 3$ ) are indicated by filled (blue) and open (green) symbols, respectively. The red filled circle denotes the Sun. For BD+44°493, where the S I lines are invisible, the upper limit values corresponding to  $EW_{10455} \leq 4 \text{ m}\AA$  (cf. subsection 4.1) are shown by filled (pink) triangles.

relevant data (including  $EW$  and  $\Delta$  for all three lines and each of the  $\delta$  values) are presented in electronic table E2.

## 5. Discussion

### 5.1. Behavior of $[S/Fe]$ against $[Fe/H]$

The  $[S/Fe]$  vs.  $[Fe/H]$  relation resulting from this investigation is shown in figure 3a. A significant characteristic read from this figure is that the  $[S/Fe]$  ratio attains considerably high values ( $\sim +0.7$ – $0.8$  dex) in very metal-poor halo stars with  $[Fe/H] \sim -3$  (such as G 64-37, BD-18°5550, and HD 115444). The upper limit of  $[S/Fe]$  ( $\leq +1.0$ ) for BD+44°493 ( $[Fe/H] \simeq -3.7$ ) does not contradict this argument. It should be noted that this is a result after taking into account the negative (downward) non-LTE correction by  $\sim 0.2$ – $0.3$  dex.<sup>5</sup> Accordingly, we

<sup>4</sup> In addition to such estimated abundance ambiguities due to errors in the adopted atmospheric parameters, we should keep in mind that uncertainties caused by photometric random errors may become significant, especially for the case of very weak lines near to the detection limit. For estimating these errors, we may invoke the formula derived by Cayrel (1988), who showed that the ambiguity in  $EW$  is roughly expressed as  $\sim 1.6(w \delta x)^{1/2} \epsilon$ , where  $w$  is the typical line FWHM,  $\delta x$  is the pixel size (in unit of wavelength), and  $\epsilon$  is the photometric accuracy represented by  $\sim (S/N)^{-1}$ . Substituting  $w \sim 0.5$ – $1 \text{ \AA}$ ,  $\delta x \simeq 0.25 \text{ \AA}$ , and  $\epsilon \sim 1/100$ , we obtain  $\sim 6$ – $8 \text{ m}\AA$  as the typical uncertainty in  $EW$ . This means that the S abundance derived for very metal-poor stars where the  $EW$  of the strongest S I line ( $EW_{10455}$ ) is around  $\sim 10 \text{ m}\AA$  could be subject to additional ambiguities due to photometric errors which may amount to  $\lesssim 0.2$ – $0.3$  dex.

<sup>5</sup> Along with the non-LTE correction, we should also pay attention to the 3D correction, since our analysis is based on Kurucz’s (1993) 1D model atmospheres. Caffau et al. (2007) theoretically investigated the 3D effect on S abundance determinations for



conclude that the behavior of [S/Fe] is different from the “flat” trend exhibited by other refractory  $\alpha$ -elements (e.g., Mg, Si, Ca, Ti) showing only moderately supersolar  $[\alpha/\text{Fe}]$  ratio of  $\sim +0.3$ – $0.5$  dex at the metal-deficient regime between  $[\text{Fe}/\text{H}] \sim -2$  and  $\sim -4$  (e.g., Cayrel et al. 2004). Such a difference in  $[\alpha/\text{Fe}]$  behavior at the very low-metallicity region between refractory and volatile species may pose a significant observational constraint on the chemical evolution in the early-time of the Galaxy (e.g., a necessity of including the effect of time-delayed deposition).

It should be stressed here, however, that [S/Fe] never simply keeps rising up to such a large value with a decrease in  $[\text{Fe}/\text{H}]$ , as previously argued. The behavior of [S/Fe] at  $-3 \lesssim [\text{Fe}/\text{H}] \lesssim 0$  we found here is actually more complicated: After a gradual rise from  $[\text{Fe}/\text{H}] \sim 0$  to  $\sim -1$  (the typical tendency seen in  $\alpha$  elements), a local plateau (or even a slight downward bending) is recognized at  $-2.5 \lesssim [\text{Fe}/\text{H}] \lesssim -1.5$  with a mildly supersolar [S/Fe] ( $\sim +0.3$ ), which then experiences a sudden jump between the narrow interval at  $-3 \lesssim [\text{Fe}/\text{H}] \lesssim -2.5$  up to [S/Fe]  $\sim +0.7$ – $0.8$  at  $[\text{Fe}/\text{H}] \sim -3$ . Thus, to say the least, the behavior of [S/Fe] is rather intricate with a zigzag appearance, which is neither globally flat nor monotonically increasing. This is the consequence of this study.

### 5.2. Comparison with the Results from Different Lines

In order to examine whether or not any systematic effect exists between the abundances derived from different lines, we compared the  $[\text{S}/\text{H}]_{104}$  values derived from 10455–10459 lines in this study with  $[\text{S}/\text{H}]_{92}$  (9212/9228/9237 lines) or  $[\text{S}/\text{H}]_{86}$  (8693–4 lines) taken from the published results where data for any of our targets are available. In doing this, we paid special attention to the consistency that both [S/H]’s to be compared correspond to the same atmospheric parameters ( $T_{\text{eff}}$ ,  $\log g$ , and  $v_t$ ). Regarding  $[\text{S}/\text{H}]_{92}$  (non-LTE values), the data for 5 stars (G 64-37, G 29-23, G 18-39, HD 194598, HD 193901) were taken from table 1 of Nissen et al. (2007b), while those for 6 stars (HD 122563, HD 140283, HD 108317, HD 19445, HD 201891, HD 148816) are the non-LTE reanalysis results of Takada-Hidai et al.’s (2005) equivalent widths as done by Takeda et al. (2005b; cf. subsection 4.1 therein). Meanwhile,  $[\text{S}/\text{H}]_{86}$  for 9 stars (HD 5682, HD 142373, HD 165908, HD 10700, HD 131156, HD 141004, HD 196755, HD 161797, HD 182572) were taken from Takeda (2007). Although these  $[\text{S}/\text{H}]_{86}$ ’s are LTE values, we used them as they are, since non-LTE corrections for 8693–4 lines are practically negligible; i.e., only a few hundredths dex in the case of population I dwarfs (cf. Takeda et al. 2005b). The resulting  $[\text{S}/\text{H}]_{92}^{\text{NLTE}}$

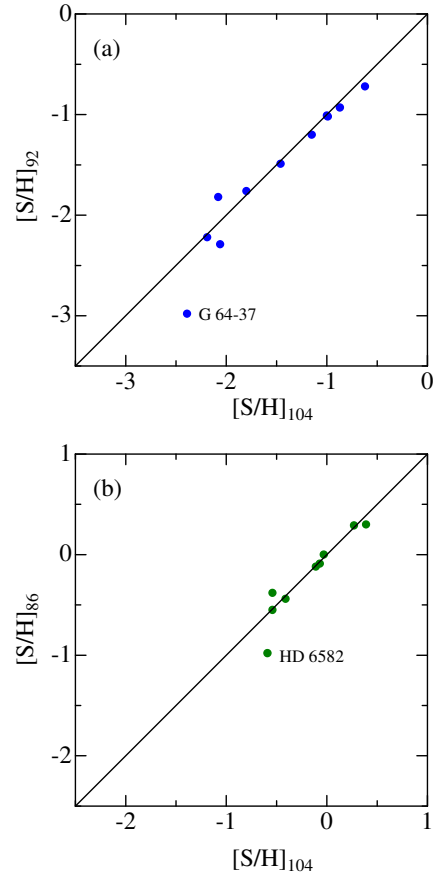


**Fig. 4.** Correlation of “star–Sun” sulfur abundance difference determined in this study based on S I 10455–10459 lines of multiplet 3 ( $[\text{S}/\text{H}]_{104}$ ) with those derived from other S I lines with the same atmospheric parameters as adopted in this study. (a) Comparison with  $[\text{S}/\text{H}]_{92}$  derived from S I 9212/9228/9237 lines of multiplet 2 for 11 stars in common (based on the data published by Takada-Hidai et al. 2005 and Nissen et al. 2007b) (b) Comparison with  $[\text{S}/\text{H}]_{86}$  derived from S I 8693–4 lines of multiplet 6 for 9 stars in common (based on the results obtained by Takeda 2007). See subsection 5.2 for more details.

vs.  $[\text{S}/\text{H}]_{104}^{\text{NLTE}}$  and  $[\text{S}/\text{H}]_{86}^{\text{LTE}}$  vs.  $[\text{S}/\text{H}]_{104}^{\text{NLTE}}$  correlation plots are shown in figures 4a and b, respectively. We can see from these figures that the agreement is fairly good in most cases, though exceptionally large deviation is seen at the low abundance end for each panel (G 64-37 and HD 6582).

Regarding HD 6582, the reason for the disagreement ( $\sim 0.4$  dex) between  $[\text{S}/\text{H}]_{104}^{\text{NLTE}}$  ( $-0.59$ ; this study) and  $[\text{S}/\text{H}]_{86}^{\text{LTE}}$  ( $-0.98$ ; Takeda 2007) is well understandable. This is due to the fact that the S I 8693–4 feature for this star is too weak (because of its low metallicity nature) to yield a reliable S abundance, as can be recognized from figure 4 of Takeda (2007). Therefore,  $[\text{S}/\text{H}]_{86}$  should be regarded as erroneous for this case of HD 6582. Considering the satisfactory agreement between  $[\text{S}/\text{H}]_{86}^{\text{LTE}}$  and  $[\text{S}/\text{H}]_{104}^{\text{NLTE}}$  for the other stars, we may state that S I 10455–10459 lines can be a useful S abundance indicator also for comparatively metal-rich population I stars, if

FGK population I dwarfs (including the Sun), and found that the 3D corrections for the solar S I 10455–10459 lines are on the order of  $+0.1$  dex (cf. their table 2). Meanwhile, according to the recent work of Caffau et al. (2010), the 3D corrections for the S abundances of metal-poor stars derived from S I 10455–10459 lines are again  $\sim +0.1$  dex (cf. their table 4). Therefore, we can reasonably assume that the 3D effect is insignificant for [S/Fe] (where “relative” abundance between a star and the Sun is involved) because of being canceled.

non-LTE corrections are properly taken into account.

On the other hand, the large discrepancy amounting to  $\sim 0.6$  dex shown by of G 64-37 ( $[\text{S}/\text{H}]_{92}^{\text{NLTE}} = -2.98$  and  $[\text{S}/\text{H}]_{104}^{\text{NLTE}} = -2.39$ ) is more serious and puzzling. Admittedly, our abundance result for this star may be subject to comparatively large uncertainty because its spectrum quality is not sufficiently good for measuring very weak lines (cf. figure 2). However, we consider that at least its detection is probably real; so the abundance of this star being lower by  $\sim 0.6$  dex is rather hard to accept. At any rate, if Nissen et al.’s (2007b) low-scale result is correct, it has an important implication that  $[\text{S}/\text{Fe}]$  as low as  $\sim +0.1$  does exist at  $[\text{Fe}/\text{H}] \sim -3$ , which does not match our consequence.

Given the general agreement between  $[\text{S}/\text{Fe}]_{104}^{\text{NLTE}}$  and  $[\text{S}/\text{Fe}]_{92}^{\text{NLTE}}$ , we consider that the flat (or slightly bending) trend of  $[\text{S}/\text{Fe}]_{92}^{\text{NLTE}}$  at  $\sim +0.2$  derived by Nissen et al. (2007b; cf. the lower panel of their figure 11) is reasonable (at least at  $-2.7 \lesssim [\text{Fe}/\text{H}] \lesssim -1$ ), in the sense that it may correspond to the local plateau we found for  $[\text{S}/\text{Fe}]_{104}^{\text{NLTE}}$  at  $-2.5 \lesssim [\text{Fe}/\text{H}] \lesssim -1.5$ . However, their low  $[\text{S}/\text{Fe}]_{92}^{\text{NLTE}}$  results of  $\sim +0.1$ – $0.3$  for all three stars at  $[\text{Fe}/\text{H}] \sim -3$  are difficult to interpret, because of being discordant with what we found from  $[\text{S}/\text{Fe}]_{104}^{\text{NLTE}}$ . Depending on cases, it might be necessary to abandon the idea that almost unique  $[\text{S}/\text{Fe}]$  should correspond to a given  $[\text{Fe}/\text{H}]$ . Namely, we may have to regard that  $[\text{S}/\text{Fe}]$  at this very low metallicity region is considerably diversified or bifurcated in the sense that stars with high- and low-scale  $[\text{S}/\text{Fe}]$  are mixed around the same  $[\text{Fe}/\text{H}]$ . As a matter of fact, Caffau et al. (2005) suggested that  $[\text{S}/\text{Fe}]$  vs.  $[\text{Fe}/\text{H}]$  relation may be bimodal in the sense that it consists of two separate sequences branching off around  $[\text{Fe}/\text{H}] \sim -1.5$  (see also Caffau et al. 2010). If this is really the case, it might suggest a difference in the degree of ISM mixing; i.e., changing from incompletely to well mixed with increasing  $[\text{Fe}/\text{H}]$  (e.g., Argast et al. 2000).

We do not insist, of course, that the behavior of  $[\text{S}/\text{Fe}]$  we concluded in this investigation (figure 3a) exclusively describes the nature of sulfur abundances of metal-poor regime applicable to all halo stars. It is clear that our object sample is still too small to extract any decisive conclusion. Obviously, further more S abundance studies on a much larger number of metal-deficient stars in a wide range of metallicity ( $-3 \lesssim [\text{Fe}/\text{H}] \lesssim -1$ ), preferably by using both S I 10455–10459 as well as 9212/9228/9237 lines, would be required to settle the problem.

## 6. Conclusion

Motivated by the recent debate on the  $[\text{S}/\text{Fe}]$  vs.  $[\text{Fe}/\text{H}]$  relation of metal-deficient stars at  $-3 \lesssim [\text{Fe}/\text{H}] \lesssim -1$ , where “rising” or “flat” tendencies have been differently suggested depending on the lines used (S I 8693–4 lines of multiplet 6 or S I 9212/9228/9237 lines of multiplet 1), we conducted an extensive abundance analysis on 33 disk/halo stars in the wide metallicity range ( $-3.6 \lesssim [\text{Fe}/\text{H}] \lesssim +0.3$ ) by using S I 10455–10459 lines of multiplet 3, a new probe potentially effective for exploring

S abundances of very metal-poor stars.

The observations were carried out in 2009 July by using IRCS+AO188 of the Subaru Telescope and spectra of sufficiently high resolution ( $R \sim 20000$ ) and high S/N ( $\sim 100$ – $200$ ) were obtained in  $zJ$ -band ( $1.04$ – $1.19 \mu\text{m}$ ). Thanks to the high quality of the data, we could successfully determine the sulfur abundances from the S I 10455–10459 triplet for most of the targets by using the non-LTE spectrum synthesis technique.

We found an evidence of considerably large  $[\text{S}/\text{Fe}]$  ratio amounting to  $\sim +0.7$ – $0.8$  dex at very low metallicity ( $[\text{Fe}/\text{H}] \sim -3$ ), which makes a marked contrast with other refractory  $\alpha$ -elements (such as Mg, Si, Ca, Ti), which are known to show a flat tendency at  $[\alpha/\text{Fe}] \sim 0.3$  over the whole halo metallicity range. Given that S is a volatile element among the  $\alpha$  group, such a difference may pose a significant constraint on the galactic chemical evolution.

The resulting global nature of  $[\text{S}/\text{Fe}]$  over the wide metallicity range is not so simple as has been argued (i.e., neither simply flat nor ever increasing) but actually rather complex: After a gradual rise from  $[\text{S}/\text{Fe}] \sim 0$  ( $[\text{Fe}/\text{H}] \sim 0$ ) to  $[\text{S}/\text{Fe}] \sim +0.3$  ( $[\text{Fe}/\text{H}] \sim -1$ ), a local plateau (or even a slight downward bending) extends over  $-2.5 \lesssim [\text{Fe}/\text{H}] \lesssim -1.5$  with a mildly supersolar  $[\text{S}/\text{Fe}]$  ( $\sim +0.3$ ), which is followed by a sudden increase between the narrow interval ( $-3 \lesssim [\text{Fe}/\text{H}] \lesssim -2.5$ ) up to  $[\text{S}/\text{Fe}] \sim +0.7$ – $0.8$  at  $[\text{Fe}/\text{H}] \sim -3$ .

We could not find any systematic difference between the abundances derived from these S I 10455–10459 lines and those from other 8693–4 or 9212/9228/9237 lines, which are mostly in agreement. We thus consider that the flat trend of  $[\text{S}/\text{Fe}]$  at  $\sim +0.2$  concluded by Nissen et al. (2007b) based on 9212/9237 lines actually correspond to the local plateau we found at  $-2.5 \lesssim [\text{Fe}/\text{H}] \lesssim -1.5$ . However, it is not clear why they did not detect such large  $[\text{S}/\text{Fe}]$  of  $\sim 0.7$ – $0.8$  as we found at  $[\text{Fe}/\text{H}] \sim -3$ . One possible explanation might be that stars with high- and low-scale  $[\text{S}/\text{Fe}]$  are mixed around the same  $[\text{Fe}/\text{H}]$ , though it has to be observationally confirmed based on a much larger sample.

We express our heartfelt thanks to Y. Minowa and T.-S. Pyo for their kind advices and helpful support in preparing as well as during the IRCS+AO188 observations.

One of the authors (M. T.-H.) is grateful for a financial support from a grant-in-aid for scientific research (C, No. 22540255) from the Japan Society for the Promotion of Science.

This research has made use of the SIMBAD database, operated by CDS, Strasbourg, France.

## Appendix. Double-Star Nature of HD 219617

In our observation by using the Subaru Telescope with IRCS+AO188, we accidentally realized that HD 219617 was a double-star with similar components, thanks to the high spatial resolution ( $\lesssim 0.''1$ ) accomplished by the adaptive optics system (AO188). Consulting the SIMBAD database, we learned that this is really a double sys-

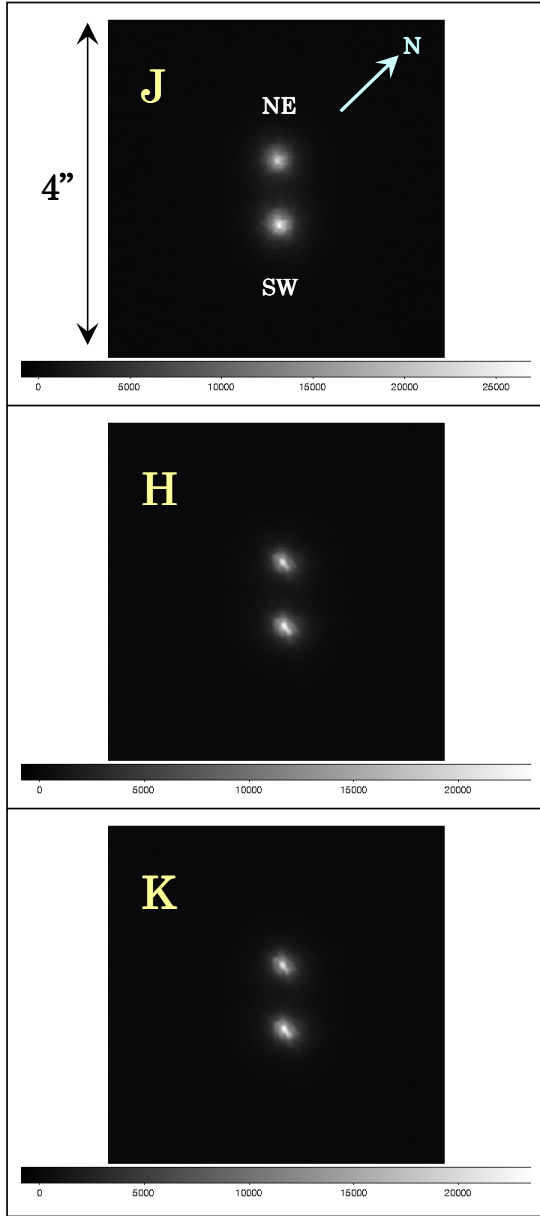


**Fig. 5.** High-resolution images of HD 219617 in *J*, *H*, and *K* bands, which were obtained in the imaging mode of IRCS+AO188.

tem (WDS 23171–1349) of  $0.''8$  separation, comprising 9.08 (*V*) and 8.77 (*V*) F8 IV stars. Since the fainter one is in the North-East direction and the brighter one is in the South-East, we call the former and the latter HD 219617 (NE) and HD 219617 (SW), respectively. We obtained its *J*-, *H*-, and *K*-band images by making use of the imaging mode of IRCS (cf. figure 5), from which we confirmed that NE is slightly fainter than SW also in near IR:  $J_{\text{NE}} - J_{\text{SW}} = +0.20$ ,  $H_{\text{NE}} - H_{\text{SW}} = +0.27$ , and  $K_{\text{NE}} - K_{\text{SW}} = +0.20$ .

Although chemical abundances of this star have been repeatedly studied by a number of investigators, the com-

bined spectrum of both components seems to have been used without attending its binary nature, presumably because these two tend to merge already in the natural seeing condition of  $\sim 1''$ – $2''$ . Since we could obtain the spectrum of each component separately, we here briefly describe the comparison of these two.

A notable characteristic is that two spectra are remarkably similar to each other, as shown in figure 6. Actually, they are hardly discernible by eyes. According to the comparison of *EW*s (from  $\sim 10$  to  $\sim 230$  mÅ) measured for 32 lines (of C I, Mg I, Si I, S I, Fe I, and Sr II), we found that the correlation is very good ( $r = 0.94$ ) and a linear regression analysis yielded  $EW_{\text{SW}} = 1.020EW_{\text{NE}} - 1.3$  (where *EW* is in unit of mÅ). Thus, almost no essential systematic difference exists in terms of the line strengths. Besides, the striking similarity of Paschen  $\gamma$  wing (figure 6b) suggests that  $T_{\text{eff}}$  is almost the same. We thus assigned the same atmospheric parameters for both NE and SW. We also point out that the radial velocity is again practically the same ( $V_{\text{rad}}^{\text{hel}}$  is  $+14$  km s $^{-1}$  and  $+13$  km s $^{-1}$  for NE and SW, respectively; cf. electronic table E1).

Accordingly, previous studies having analyzed the combined spectrum of HD 219617 as if it is a single star should have obtained almost the correct result, because each of Sp(NE), Sp(SW), Sp(NE+SW) are essentially the same. Yet, one point to notice is, that stellar parameters should not be derived from the luminosity simply estimated from the apparent (total) brightness of this double star. Fulbright (2000), who evidently treated this star as being single, initially guessed its  $\log g$  from Hipparcos parallax (i.e., via luminosity) as 3.9, while he finally adopted the spectroscopically determined  $\log g$  of 4.3. We speculate that this difference of 0.4 dex may have stemmed from the overestimation of the luminosity.

## References

- Argast, D., Samland, M., Gerhard, O. E., Thielemann, F.-K. 2000, *A&A*, 356, 873
- Caffau, E., Bonifacio, P., Faraggiana, R., François, P., Gratton, R. G., & Barbieri, M. 2005, *A&A*, 441, 533
- Caffau, E., Faraggiana, R., Bonifacio, P., Ludwig, H.-G., & Steffen, M. 2007, *A&A*, 470, 699
- Caffau, E., Sbordone, L., Ludwig, H.-G., Bonifacio, P., & Spite, M. 2010, *Astron. Nachr.*, 331, 725
- Castelli, F., Gratton, R. G., & Kurucz, R. L. 1997, *A&A*, 318, 841
- Cayrel, R. 1988, in *Proc. IAU Symp. 132, The Impact of Very High S/N Spectroscopy on Stellar Physics*, ed. G. Cayrel de Strobel & M. Spite (Dordrecht: Kluwer), 345
- Cayrel, R., et al. 2004, *A&A*, 416, 1117
- Fulbright, J. P. 2000, *ApJ*, 120, 841
- Ibukiyama, A., & Arimoto, N. 2002, *A&A*, 394, 927
- Israelian, G., & Rebolo, R. 2001, *ApJ*, 557, L43
- Ito, H., Aoki, W., Honda, S., & Beers, T. C. 2009, *ApJ*, 698, L37
- Kobayashi, N., et al. 2000, *Proc. SPIE*, 4008, 1056
- Korotin, S. A. 2009, *Astron. Rep.* 53, 651
- Kurucz, R. L. 1993, *Kurucz CD-ROM*, No. 13 (Harvard-Smithsonian Center for Astrophysics)

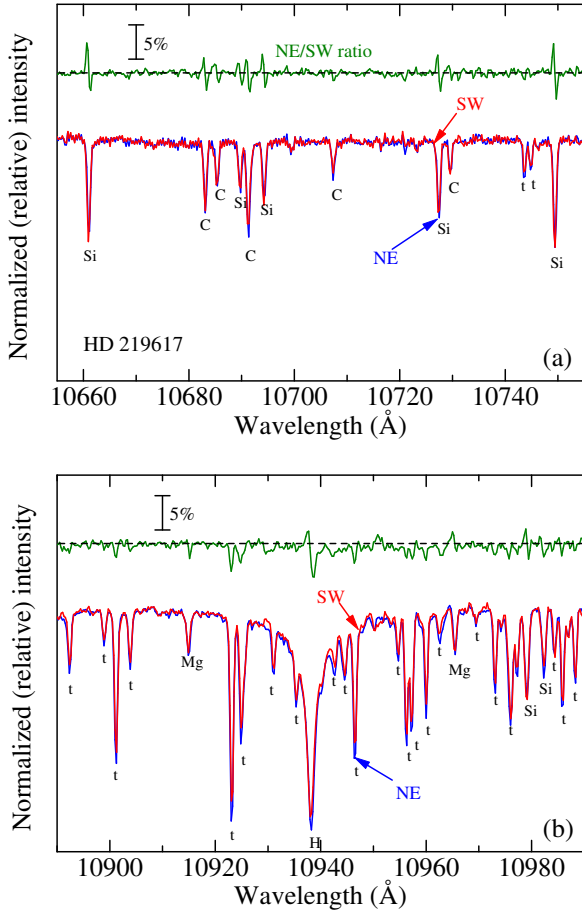


**Fig. 6.** Comparison of the spectra of HD 219617(NE) and HD 219617(SW). (a) 10655–10755 Å region comprising C I and Si I lines, (b) 10890–10990 Å region comprising the conspicuous Paschen  $\gamma$  line of neutral hydrogen. Though these two spectra are depicted in different colors (NE in blue and SW in red), they are hardly discernible when overlapped. The NE/SW spectrum residuals (NE divided by SW) are also displayed in each panel to demonstrate their remarkable similarity. Note that many lines in panel (b) are telluric water vapor lines (denoted as “t”). The wavelength scale of each spectrum has been adjusted to the laboratory frame.

- Kurucz, R. L., & Bell, B. 1995, Kurucz CD-ROM, No. 23 (Harvard-Smithsonian Center for Astrophysics)
- Kurucz, R. L., Furenlid, I., Brault, J., & Testerman, L. 1984, Solar Flux Atlas from 296 to 1300 nm (Sunspot, New Mexico: National Solar Observatory)
- Leushin, V. V., & Topil'skaya, G. P. 1986, *Astrophysics*, 25, 415
- Nissen, P. E., Asplund, M., Fabbian, D., Kerber, F., Käufel, H. U., & Pettini, M. 2007a, *Messenger*, 128, 38
- Nissen, P. E., Akerman, C., Asplund, M., Fabbian, D., Kerber, F., Käufel, H. U., & Pettini, M. 2007b, *A&A*, 469, 319
- Nissen, P. E., Akerman, C., Asplund, M., Fabbian, D., & Pettini, M. 2008, in *Precision Spectroscopy in Astrophysics*, eds. N. C. Santos, L. Pasquini, A. C. M. Correia, & M. Romaniello, (Garching, Germany: ESO), 51
- Nissen, P. E., Chen, Y. Q., Asplund, M., & Pettini, M. 2004, *A&A*, 415, 993
- Ramaty, R., Lingenfelter, R. E., & Kozlovsky, B. 2001, *NewAR*, 45, 587
- Ryde, N., & Lambert, D. L. 2004, *A&A*, 415, 559
- Simmerer, J., Sneden, C., Cowan, J. J., Collier, J., Woolf, V. M., & Lawler, J. E. 2004, *ApJ*, 617, 1091
- Takada-Hidai, M., Saito, Y., Takeda, Y., Honda, S., Sadakane, K., Masuda, S., & Izumiura, H. 2005, *PASJ*, 57, 347
- Takada-Hidai, M., & Sargent, W. L. W. 2005, in *From Lithium to Uranium: Elemental Tracers of Early Cosmic Evolution*, IAU Symposium 228, eds. V. Hill, P. François, & F. Primas, (Cambridge: Cambridge University Press), 277
- Takada-Hidai, M., Takeda, Y., Sato, S., Honda, S., Sadakane, K., Kawanomoto, S., Sargent, W. L. W., Lu, L., & Barlow, T. A. 2002, *ApJ*, 573, 614
- Takeda, Y. 1995, *PASJ*, 47, 287
- Takeda, Y. 2007, *PASJ*, 59, 335
- Takeda, Y., Hashimoto, O., Taguchi, H., Yoshioka, K., Takada-Hidai, M., Sato, Y., & Honda, S. 2005b, *PASJ*, 57, 751
- Takeda, Y., Kaneko, H., Matsumoto, N., Oshino, S., Ito, H., & Shibuya, T. 2009, *PASJ*, 61, 563
- Takeda, Y., Ohkubo, M., Sato, B., Kambe, E., & Sadakane, K. 2005a, *PASJ*, 57, 27 [Erratum: 57, 415]
- Tokunaga, A. T., et al. 1998, *Proc. SPIE*, 3354, 512



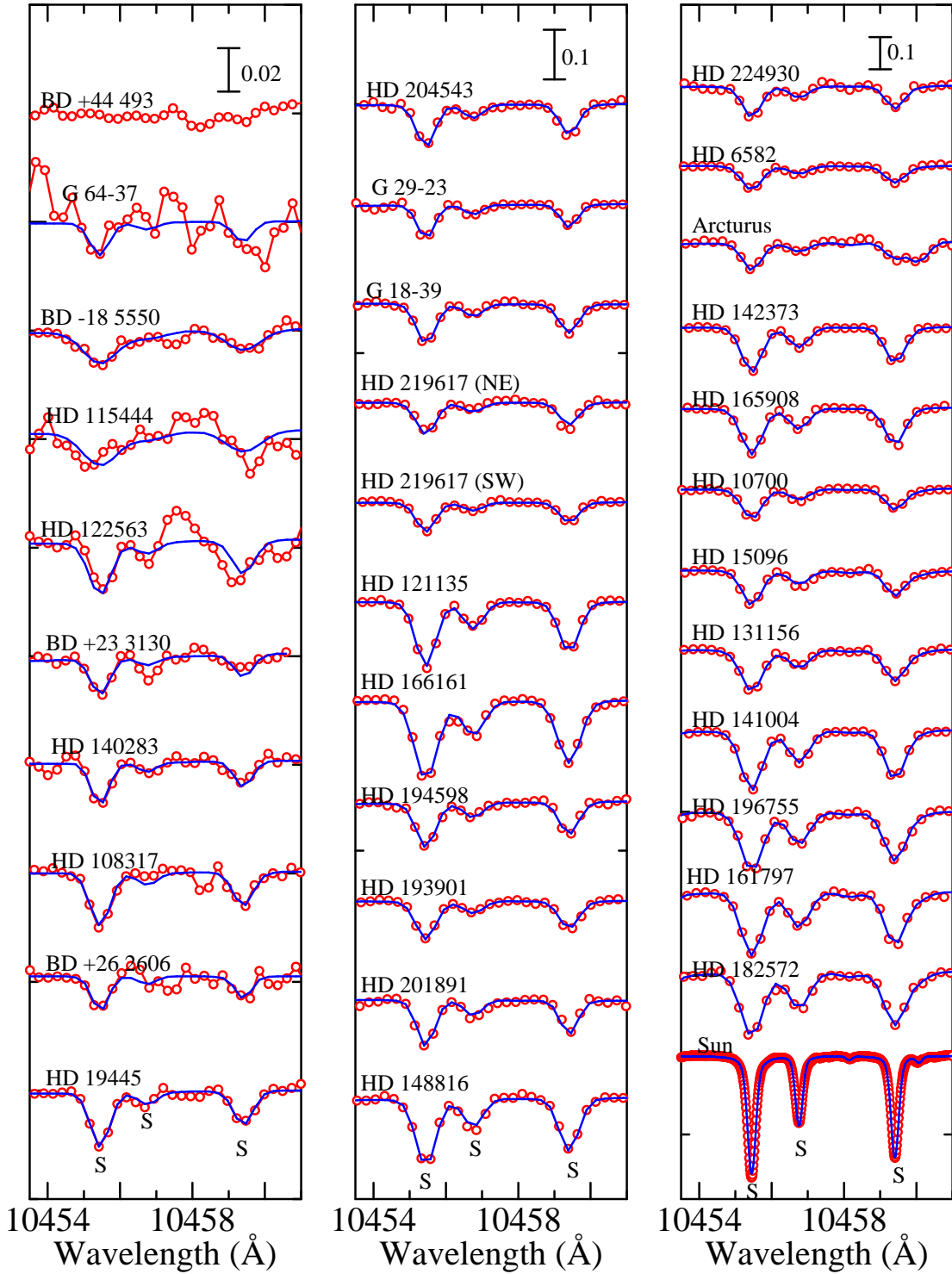


**Fig. 2.** Synthetic spectrum fitting for the S I 10455–10459 triplet lines. The best-fit theoretical spectra are shown by (blue) solid lines, while the observed data are plotted by (red) symbols. In each panel (from left to right), the spectra are arranged (from top to bottom) in the ascending order of [Fe/H] as in table 1. An appropriate vertical offset (0.05, 0.2, 0.25 for the left, middle, and right panel, respectively) is applied to each spectrum relative to the adjacent one. The wavelength scale of each spectrum has been adjusted to the laboratory frame.

**Table 1.** Parameters of the program stars and the results of abundance analyses.

| Name          | $T_{\text{eff}}$<br>(K) | $\log g$<br>( $\text{cm s}^{-2}$ ) | $v_t$<br>( $\text{km s}^{-1}$ ) | [Fe/H]<br>(dex) | Ref.  | $A^{\text{N}}$<br>(dex) | $EW_{10455}$<br>(mÅ) | $\Delta_{10455}$<br>(dex) | [S/Fe]<br>(dex) | Remark                                     |
|---------------|-------------------------|------------------------------------|---------------------------------|-----------------|-------|-------------------------|----------------------|---------------------------|-----------------|--|
| BD+44°493     | 5510                    | 3.70                               | 1.30                            | −3.68           | ITO09 | 4.49                    | ( $\leq 4$ )         | (−0.34)                   | ( $\leq +1.0$ ) | S lines unmeasurable<br>larger uncertainty |
| G 64-37       | 6432                    | 4.24                               | 1.50                            | −3.08           | NIS07 | 4.81                    | 9.9                  | −0.26                     | +0.69           |  |
| BD−18°5550    | 4750                    | 1.40                               | 1.80                            | −3.06           | CAY04 | 4.90                    | 16.7                 | −0.25                     | +0.76           |  |
| HD 115444     | 4721                    | 1.74                               | 2.00                            | −2.71           | SIM04 | 5.15                    | 17.9                 | −0.18                     | +0.66           |  |
| HD 122563     | 4572                    | 1.36                               | 2.90                            | −2.61           | SIM04 | 5.13                    | 18.4                 | −0.16                     | +0.54           |  |
| BD+23°3130    | 5000                    | 2.20                               | 1.40                            | −2.60           | FUL00 | 4.86                    | 10.6                 | −0.19                     | +0.26           |  |
| HD 140283     | 5830                    | 3.67                               | 1.90                            | −2.55           | MTH05 | 5.01                    | 12.0                 | −0.18                     | +0.36           |  |
| HD 108317     | 5310                    | 2.77                               | 1.90                            | −2.35           | MTH05 | 5.12                    | 16.9                 | −0.18                     | +0.27           |  |
| BD+26°2606    | 5875                    | 4.10                               | 0.40                            | −2.30           | FUL00 | 5.10                    | 9.8                  | −0.09                     | +0.20           |  |
| HD 19445      | 6130                    | 4.39                               | 2.10                            | −2.05           | MTH05 | 5.40                    | 17.2                 | −0.08                     | +0.25           |  |
| HD 204543     | 4672                    | 1.49                               | 2.00                            | −1.72           | SIM04 | 5.85                    | 53.3                 | −0.20                     | +0.37           |  |
| G 29-23       | 6194                    | 4.04                               | 1.50                            | −1.69           | NIS07 | 5.74                    | 39.6                 | −0.11                     | +0.23           |  |
| G 18-39       | 6093                    | 4.19                               | 1.50                            | −1.46           | NIS07 | 6.05                    | 54.0                 | −0.10                     | +0.31           |  |
| HD 219617(NE) | 5825                    | 4.30                               | 1.40                            | −1.40           | FUL00 | 6.07                    | 43.8                 | −0.06                     | +0.27           | North-East component                       |
| HD 219617(SW) | 5825                    | 4.30                               | 1.40                            | −1.40           | FUL00 | 6.00                    | 39.3                 | −0.06                     | +0.20           | South-West component                       |
| HD 121135     | 4934                    | 1.91                               | 1.60                            | −1.37           | SIM04 | 6.30                    | 89.0                 | −0.29                     | +0.47           |  |
| HD 166161     | 5350                    | 2.56                               | 2.25                            | −1.22           | SIM04 | 6.44                    | 120.8                | −0.32                     | +0.46           |  |
| HD 194598     | 6020                    | 4.30                               | 1.40                            | −1.15           | NIS07 | 6.21                    | 59.6                 | −0.08                     | +0.16           |  |
| HD 193901     | 5699                    | 4.42                               | 1.20                            | −1.10           | NIS07 | 6.33                    | 53.0                 | −0.05                     | +0.23           |  |
| HD 201891     | 5900                    | 4.19                               | 1.40                            | −1.10           | MTH05 | 6.20                    | 57.2                 | −0.08                     | +0.10           |  |
| HD 148816     | 5860                    | 4.07                               | 1.60                            | −1.00           | MTH05 | 6.58                    | 93.7                 | −0.12                     | +0.38           |  |
| HD 224930     | 5275                    | 4.10                               | 1.05                            | −0.90           | FUL00 | 6.65                    | 60.5                 | −0.05                     | +0.35           |  |
| HD 6582       | 5331                    | 4.54                               | 0.73                            | −0.81           | TAK05 | 6.61                    | 49.6                 | −0.03                     | +0.22           |  |
| Arcturus      | 4281                    | 1.72                               | 1.49                            | −0.55           | TAK09 | 6.66                    | 42.0                 | −0.15                     | +0.01           |  |
| HD 142373     | 5776                    | 3.83                               | 1.26                            | −0.51           | TAK05 | 6.66                    | 96.2                 | −0.15                     | −0.03           |  |
| HD 165908     | 6183                    | 4.35                               | 1.24                            | −0.46           | TAK05 | 6.66                    | 100.2                | −0.12                     | −0.08           |  |
| HD 10700      | 5420                    | 4.68                               | 0.66                            | −0.43           | TAK05 | 6.79                    | 59.4                 | −0.03                     | +0.02           |  |
| HD 15096      | 5375                    | 4.30                               | 0.80                            | −0.20           | FUL00 | 6.87                    | 66.7                 | −0.06                     | −0.13           |  |
| HD 131156     | 5527                    | 4.60                               | 1.10                            | −0.13           | TAK05 | 7.09                    | 90.5                 | −0.06                     | +0.02           |  |
| HD 141004     | 5877                    | 4.11                               | 1.17                            | −0.01           | TAK05 | 7.13                    | 134.2                | −0.15                     | −0.06           |  |
| HD 196755     | 5750                    | 3.83                               | 1.23                            | +0.09           | TAK05 | 7.17                    | 138.5                | −0.17                     | −0.12           |  |
| HD 161797     | 5580                    | 3.99                               | 1.11                            | +0.29           | TAK05 | 7.47                    | 146.7                | −0.14                     | −0.02           |  |
| HD 182572     | 5566                    | 4.11                               | 1.07                            | +0.33           | TAK05 | 7.59                    | 155.1                | −0.13                     | +0.06           |  |
| Sun           | 5780                    | 4.44                               | 1.00                            | 0.00            | ...   | 7.20                    | 122.4                | −0.10                     | 0.00            |  |

In columns 1 through 6 are given the star designation, effective temperature, logarithmic surface gravity, microturbulent velocity dispersion, Fe abundance relative to the Sun, and key for the reference of atmospheric parameters: ITO09 ... Ito et al. (2009), NIS07 ... Nissen et al. (2007b), CAY04 ... Cayrel et al. (2004), SIM04 ... Simmerer et al. (2004), FUL00 ... Fulbright (2000), MTH05 ... Takada-Hidai et al. (2005), TAK05 ... Takeda et al. (2005a), TAK09 ... Takeda et al. (2009). Columns 7–10 present the results of the abundance analysis.  $A^{\text{N}}$  is the non-LTE logarithmic abundance of S (in the usual normalization of  $H = 12.00$ ) derived from spectrum-synthesis fitting,  $EW_{10455}$  is the equivalent width (in mÅ) for the S I 10455 line inversely computed from  $A^{\text{N}}$ ,  $\Delta_{10455}$  is the non-LTE correction ( $\equiv A^{\text{N}} - A_{10455}^{\text{L}}$ ) for the S I 10455 line, and [S/Fe] ( $\equiv A^{\text{N}} - 7.20 - [\text{Fe}/\text{H}]$ ) is the S-to-Fe logarithmic abundance ratio relative to the Sun. Since HD 219617 is a double-star system (0.''8 separation) comprising two very similar stars, we assigned the same atmospheric parameters to both components (cf. the Appendix). The objects are arranged in the ascending order of [Fe/H].

**Table 2.** Atomic data of S I 10455–10458 triplet lines.

| Mult. No. | Transition                | $\lambda$ (Å) | $\chi$ (eV) | $\log gf$ | Gammar | Gammas | Gammaw |
|-----------|---------------------------|---------------|-------------|-----------|--------|--------|--------|
| 3         | $4s\ ^3S_1^o - 4p\ ^3P_2$ | 10455.45      | 6.86        | +0.26     | 8.86   | −5.21  | −7.57* |
| 3         | $4s\ ^3S_1^o - 4p\ ^3P_0$ | 10456.76      | 6.86        | −0.43     | 8.86   | −5.21  | −7.57* |
| 3         | $4s\ ^3S_1^o - 4p\ ^3P_1$ | 10459.41      | 6.86        | +0.04     | 8.86   | −5.21  | −7.57* |

Note.

These data are were taken from Kurucz and Bell's (1995) compilation. In the last three columns are given the damping parameters in the c.g.s. unit: Gammar is the radiation damping constant,  $\log \gamma_{\text{rad}}$ . Gammas is the Stark damping width per electron density at  $10^4$  K,  $\log(\gamma_e/N_e)$ . Gammaw is the van der Waals damping width per hydrogen density at  $10^4$  K,  $\log(\gamma_w/N_H)$ .

\* Computed as default values in the Kurucz's WIDTH program (cf. Leusin & Tepil'skaya 1985).